33rd Annual International Conference of the IEEE EMBS
Boston, Massachusetts USA, August 30 - September 3, 2011

Improvements in Design of Spectra of Multisine and Binary Excitation Signals for Multi-frequency Bioimpedance Measurement

Raul Land, Brian P. Cahill, Toomas Parve, *Member, IEEE*, Paul Annus, and Mart Min, *Member, IEEE*

***Abstract*—The paper discusses the usability of multi-frequency binary waveforms for broadband excitation in fast measurements of impedance spectrum of biological objects. It is shown that up to 70% of the energy of the amplitude spectrum of such two-level binary signals can be concentrated into the selected separate frequencies. The levels of selected frequency components are controllable in tens and hundreds of times. In this way we can underline the most important frequencies enhancing the corresponding amplitudes in the spectrum of excitation signal. As an implementation example, we consider the impedance spectroscopy in micro-fluidic devices for inline measurement of the conductivity of droplets in segmented flow. We use a thin-walled glass capillary with electrodes contacting the outer surface so that the contactless measurement of conductivity of liquid with biologic cells becomes possible.**

I. Introduction

ELECTRICAL bioimpedance spectra can be used to characterize the structure of living tissues and cell cultures, -- and also detect the properties of single cells can be detected. The spectra have a tendency to decrease towards higher frequencies. This means that the intensity of signals picked up from the object decreases with the frequency [1].

This decrease can be relatively small, for example, in the case of blood spectroscopy. But it can be nearly inverse proportional, as in the case of measurement of dry skin. If the frequency range of interest is significantly wide, the signal picked up from the object (the response signal) decreases tens and hundreds of times with increasing frequency. With respect to signal degradation, the signal-to-noise ratio also goes down and the exact digitizing of the response signal requires very high resolution analog-to-digital converters having from 16 to 18 bits. Using of pre-emphasized excitation signal components at the selected higher frequencies will lessen the resolution and accuracy problems in the high speed bioimpedance spectroscopy.

An example of using the impedance spectroscopy in a microfluidic device is shown in Fig. 1. In microfluidics, the most applications of impedance spectroscopy use the electrodes that have galvanic contact to the liquid that is to be measured [2]–[8]. Insulation of electrodes introduces an additional serial capacitance which greatly increases the electrode impedance. The impedance of a fast moving droplet in a high-throughput microfluidic device changes quickly, and the droplet must be transported at a high speed across the surface of the electrode without breaking up. For this reason, it is convenient that the surface of the electrode is continuous and hydrophobic. To achieve this aim, we choose to use electrodes attached to the outer surface of thin-walled (10 µm) glass capillaries (500 µm diameter). The inner surface of glass can be readily silanized with hydrophobic alkysilanes as it is common to droplet-based microfluidic systems [9], [10]. The measurement setup presented here in Fig. 1 relies therefore on electrodes that are electrically insulated.

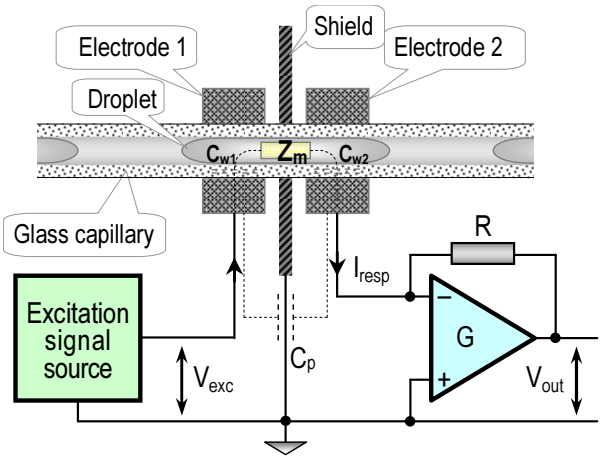

Fig. 1. Schematic diagram showing a cross-section of the micro-fluidic sensor system based on a glass capillary.

Z_m is the impedance to be measured, C_{w1} and C_{w2} are the wall capacitances between the electrodes 1 and 2 and the droplet passing through, and C_p is a shunting parallel capacitance over the shielding and between the measurement cables of an excitation signal source (generator of the voltage V_{exc}) and a converter of the response current I_{resp} to the output voltage V_{out}.

Manuscript received April 15, 2011. This work was supported in part by the European Regional Development Fund through the research centres CEBE and ELIKO.

Raul Land is with Th. J. Seebeck Department of Electronics, Tallinn University of Technology, 19086 Tallinn, Estonia, phone: +372-6202-163; (e-mail: raul@ttu.ee).

Brian P. Cahill is with the Institute for Bioprocessing and Analytical Measurement Techniques e.V., Rosenhof, Heilbad Heiligenstadt, 37308 Germany, phone: +49-3606-671-153; (e-mail: brian.cahill@iba-heiligenstadt.de).

Toomas Parve is with Th. J. Seebeck Department of Electronics, Tallinn University of Technology, 19086 Tallinn, Estonia, phone: +372-6202-160; (e-mail: parveto@elin.ttu.ee).

Paul Annus is with the Competence Centre ELIKO, 12618, Tallinn, Estonia, phone +372-6202-163; (e-mail: paul.annus@eliko.ee)

Mart Min is with Th. J. Seebeck Department of Electronics, Tallinn University of Technology, 19086 Tallinn, Estonia, phone: +372-6202-156; (e-mail: min@elin.ttu.ee).

The multi-frequency binary (+1 and -1) level voltage V_{exc} is generated by the excitation signal source and applied between the electrode 1 and ground. The excitation voltage V_{exc} causes a response current I_{resp} from the electrode 2, which corresponds to the impedance to be measured Z_m but also depends on many other parameters of the measurement set-up. The response current I_{resp} is converted in output voltage V_{out} for further digitizing and digital signal processing for information extraction. As the thickness of the insulation is much greater than the thickness of the electric double layer that forms at the surface, any effects resulting from the presence of the electric double-layer can be neglected. This work aims to lead to the measurement of the cell content of droplet-based bioreactors. Practical measurement results are shown in Fig. 2

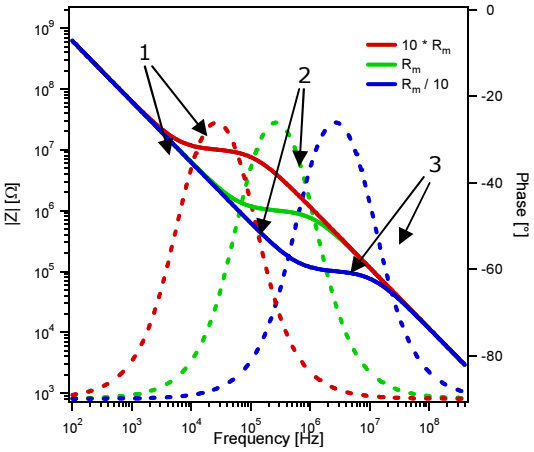

Fig. 2. The measured dependence of magnitude and phase of the impedance of microfluidic sensor (Fig. 1) on the medium resistance R_m.
Saline solution with ionic strength from 0.39 to 200 mM KCl was used in experiments. Case 1 (red curve) corresponds to $R_m = 10^7\,\Omega$, case 2 (green curve) to $10^6\,\Omega$, and case 3 (blue curve) to $10^5\,\Omega$.

II. Impedance Model

Fig. 1 shows the electrode system based on a thin-walled glass capillary. The general equivalent circuit describing this electrode system is shown in Fig. 3. The insulating wall capacitances C_{w1} and C_{w2} are given by $C_w = \varepsilon_w A/d_w$, where ε_w is the dielectric constant of the wall, A is the area of the electrode and d_w is the thickness of the wall. C_p is a parallel capacitance resulting from parasitic capacitance between the electrodes and associated cabling and from the capacitance associated with the measurement system. The impedance that is to be measured, Z_m, is the impedance of the fluid in the capillary. This is determined by the geometry of the sensor and the conductivity and dielectric constant of the fluid and is described by the medium resistance R_m and medium capacitance C_m.

In the following considerations, it is reasonable to replace the almost equal wall capacitances C_{w1} and C_{w2} with one characteristic capacitance C_w', described by the equation 1:

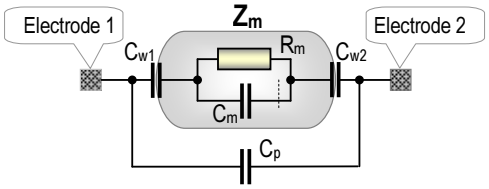

Fig. 3. Equivalent circuit diagram of the sensor system based on a glass capillary microfluidic device described in Fig. 1.
C_{w1} and C_{w2} are the capacitances between two electrodes and the droplet passing through, C_p is the shunting capacitance over the shield, and Z_m is the impedance to be measured, which consists of the resistance R_m and the capacitance C_m in parallel.

$$C_w' = \frac{C_{w1}\cdot C_{w1}}{C_{w1}+C_{w2}} \approx \frac{1}{2}\cdot\left(\frac{C_{w1}+C_{w2}}{2}\right) \tag{1}$$

The complex impedance of the whole equivalent diagram (Fig. 3) expresses as follows

$$Z(j\omega) = \frac{1}{j\omega\left(C_w' + C_p\right)}\cdot\frac{1+j\omega\left(C_m+C_w\right)R_m}{1+j\omega\left[\dfrac{C_w' C_m}{C_w'+C_p}+\dfrac{C_p\left(C_w'+C_p\right)}{C_w'+C_p}\right]R_m} \tag{2}$$

The complex impedance described by the equation (2) can be simplified using a canonic form of Laplace transform and time constants T_2 (describes a zero of the transfer function) and T_3 (describes a pole of the transfer function):

$$Z(s) = \frac{1}{sC_1}\cdot\frac{1+sT_1}{1+sT_2} \tag{3}$$

Knowing that $C_w' >> C_p$ in practical devices, we obtain the following simple equation for the complex impedance on the bases of equations (2) and (3):

$$Z(j\omega) \cong \frac{1}{j\omega C_w'}\cdot\frac{1+j\omega\left(C_m+C_w\right)R_m}{1+j\omega\left[C_m+C_p\right]R_m} \tag{4}$$

The measured capacitances $C_w' = 5$ pF, $C_p = 0.070$ pF and $C_m = 0.070$ pF, and the medium resistances $R_m = 10^7$, 10^6, and $10^5\,\Omega$ give us exactly the dependences shown in Fig. 2. The nominator of (4) characterises the first corner frequency $f_1 = 1/2\pi T_1$, and the denominator of it characterizes the second corner frequency $f_2 = 1/2\pi T_2$.

The capacitance C_w' operates as an ideal integrator: its frequency response decreases -20 dB per frequency decade and the phase lag is -90 deg. The nominator characterizes the first corner frequency $f_1 = 1/2\pi T_1$, where $T_1 = (C_m + C_w')R_m$. At the corner frequency f_1 the frequency response tends to turn to 0 dB per decade and the negative phase lag begins to reduce fast and strongly (Fig. 2).

The denominator characterises the second corner frequency $f_2 = 1/2\pi T_2$, where $T_2 = [C_m + C_p)R_m$. At this frequency the slope of the curve turns back to -20 dB per decade and the phase lag goes back towards -90 deg (Fig. 2).

To extract the values of R_m and C_m we measure the frequency responses in Fig. 2 and then will find the values of parameters through model fitting (Fig. 3).

III. Synthesis of the Excitation Signal

Multi-frequency simultaneous excitation enables the measurement time to be dramatically reduced through the measurement of impedance spectrum at all the frequency components in parallel. Binary multi-frequency excitation has been chosen for simplicity and for obtaining higher excitation energy. Because the frequency response of the impedance reduces thousands of times within the overall frequency range (Fig. 2), the level of higher frequency response signals remains significantly lower the noise level and measurement uncertainty will be very high. Therefore, the levels of separate signal components in the excitation spectrum must grow proportionally to the decrease of the response signal components (Fig. 4).

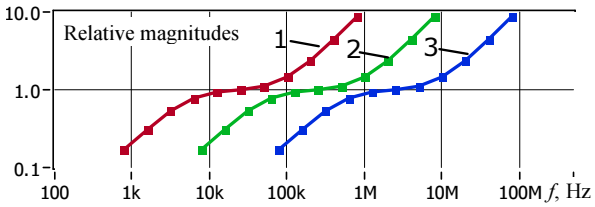

Fig. 4. The level growth functions of signal components in the multi-frequency binary excitation with the aim to cope the decrease of the response signals at higher frequencies (Fig. 2).
Case 1 (red curve) is normalized in relation to $R_m = 10^7\ \Omega$, case 2 (green curve) – to $10^6\ \Omega$, and case 3 (blue curve) – to $10^5\ \Omega$.

An inverse frequency response (Fig. 5) normalized against the dependences in Fig. 4 was designed as the basis for the synthesis of levels for the components of excitation signal.

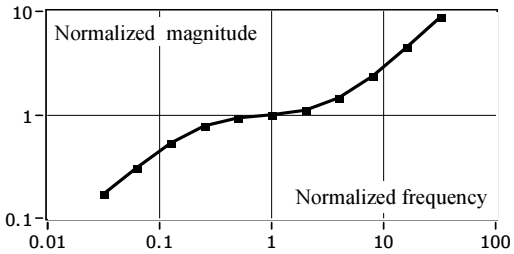

Fig. 5. The normalized inverse frequency response function generated for synthesizing the desired amplitudes of frequency components in the excitation signal.

Fig. 6 describes the synthesized binary signal containing the spectrum of components given in Fig. 7.

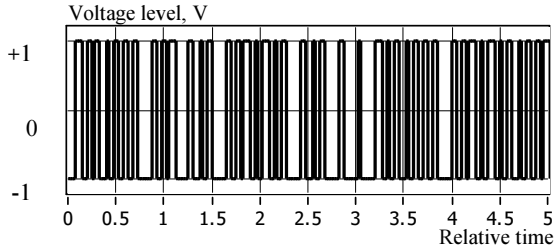

Fig. 6. Binary waveform of the synthesized multi-frequency excitation with voltage levels +1 and –1 V during its first 5 percent time section of the whole duration of the excitation signal.

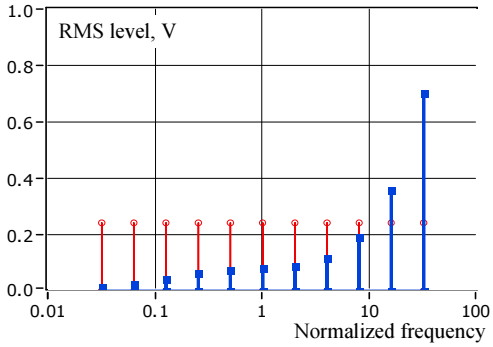

Fig. 7. The amplitude spectrum of the desired signal components (blue lines with rectangles) in the synthesized excitation signal drawn in Fig. 6, which is given in the background of equal distribution of amplitudes of the spectral components (red lines with rings).

Fig. 7 demonstrates the spectral content of the synthesized excitation (Fig. 6) with growing levels at higher frequencies drawn on the background of equal level spectrum with the RMS value of 0.24 V. The RMS level of the highest frequency component is about 0.71 V.

Fig. 8 shows that accuracy of synthesizing is accurate, only small deviations can be seen (maximally +1.5%).

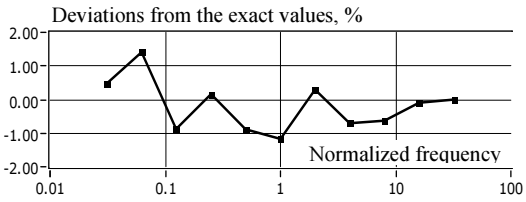

Fig. 8. A diagram with relative deviations of the amplitudes of spectral components (Fig. 7) of the synthesized binary excitation (Fig. 6) from the exact values determined by the function in Fig. 5.

Fig. 9 describes the whole spectrum of the multi-frequency binary signal characterized with the waveform in Fig. 6 and the spectral components in Fig. 7.

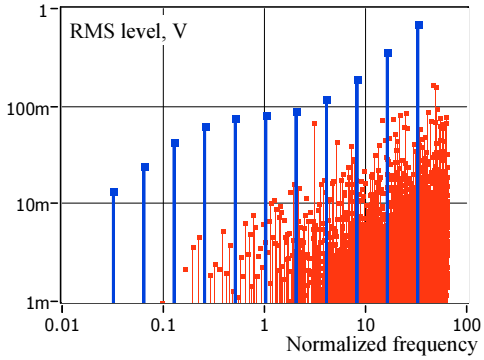

Fig. 9. Full spectrum of the generated excitation signal given in Fig 6, which contains also unusable pseudorandom components (fine red lines) in addition to the desired components (solid blue lines).

The spectrum in Fig. 9 is given in fully logarithmic scale and characterizes also those spectral components, which remain aside from the preselected ones. The role of these unusable signal components forms about 30% of the whole generated excitation signal.

IV. Conclusion

Multi-frequency sine wave excitation enlarges the possibilities for performing fast impedance spectroscopy because the measurement processes run in parallel at several frequencies [11]–[14]. Multi-frequency binary signals are not only simpler to generate but their useful energy level is also higher than their sine wave based counterparts have [11], [12], [15]–[17]. Fig. 10 characterizes uncertainties in the case when the same level (0.24 V) signal components are used in the multi-frequency binary excitation (Fig. 7). Gaussian noise level is expected to be 0.1 % RMS of the full scale 1 V. The line 2 describes the binary excitation and the line 1 characterizes multi-frequency sine wave excitation in the same conditions. It can be understood, that the uncertainty from the additive noise is about three times higher in the sine wave case. It can also be seen that the relative uncertainties can exceed 10 % line at higher frequencies.

Fig. 11 summarizes the results when non uniform levels are used for separate signal components. Uncertainty is about 4.5 % in average when the binary excitation is used, and about two times more when the multi-frequency sine wave is in use.

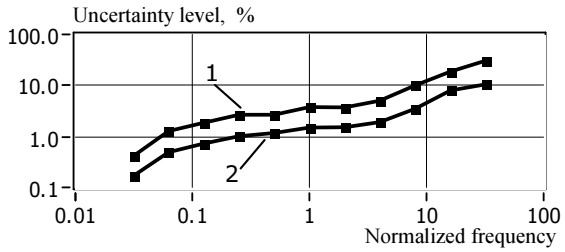

Fig. 10. Frequency dependence of uncertainties caused by the Gaussian noise of 0.1 % of the full scale in the case of equal level excitation components (Fig. 7).
Line 1 characterizes the multi-sine excitation;
Line 2 characterizes the multi-frequency binary excitation.

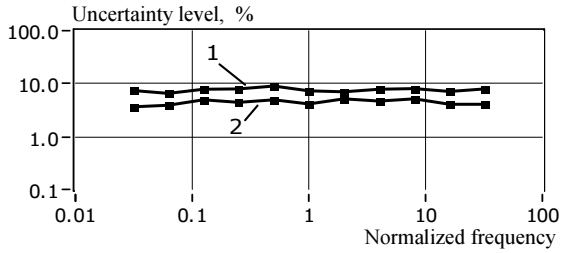

Fig. 11. Frequency dependence of uncertainties caused by the Gaussian noise of 0.1% of the full scale in the case of synthesized unequal level excitation components (Fig. 7 and Fig. 9).
Line 1 characterizes the multi-sine excitation;
Line 2 characterizes the multi-frequency binary excitation.

The paper shows that the inline impedance measurement of the conductivity of droplets in a segmented-flow system can be implemented successfully. This system is of significance for measurement of the content of droplets that are used as bioreactors in segmented flow in a micro-fluidic system. Multi-frequency binary excitation has clear advantages in high speed impedance spectroscopy.

Acknowledgment

Authors would like to thank the colleagues from Tallinn University of Technology, Tallinn, Estonia, and from the Institute for Bioprocessing and Analytical Measurement Techniques, Heilbad Heiligenstadt, Germany, for their help in manufacturing the laboratory set-ups and making experiments.

References

[1] S. Grimnes, O. G. Martinsen, *Bioimpedance and Bioelectricity Basics,* London, UK: Academic Press, 2008, 2nd ed.

[2] M. J. Schertzer, R. Ben-Mrad and P. E. Sullivan, "Using capacitance measurements in EWOD devices to identify fluid composition and control droplet mixing," *Sensors Actuators* B: *Chem*., vol. 145, pp. 340–347, 2010.

[3] U. Pliquett, D. Frense, M. Schönfeldt, C. Frätzer, Y. Zhang, B. Cahill, M. Metzen, A. Barthel, T. Nacke and D. Beckmann, "Testing miniaturized electrodes for impedance measurements within the β-dispersion – a practical approach," *J. Electr. Bioimp*., vol. 1, pp. 41–55, 2010.

[4] J. R. Burns and C. Ramshaw, "The intensification of rapid reactions in multiphase systems using slug flow in capillaries", *Lab Chip*, vol. 1, pp. 10–15, 2001.

[5] M. C. Hofmann, M. Funke, J. Büchs, W. Mokwa and U. Schnakenberg, "Development of a four electrode sensor array for impedance spectroscopy in high content screenings of fermentation processes," *Sensors Actuators* B: *Chem*., vol. 147, pp. 93–99, 2010.

[6] E. E. Krommenhoek, J. G. E. Gardeniers, J. G. Bomera, A. v. d. Berg, X. Li, M. Ottens, L. A. M. v. d. Wielen, G. W. K. v. Dedemb, M. v. Leeuwen, W. M. v. Gulik and J. J. Heijnen, "Monitoring of yeast cell concentration using a micromachined impedance sensor," *Sensors Actuators* B: *Chem*, vol. 115, pp. 384–389, 2006.

[7] H. E. Ayliffe, A. B. Frazier and R. D. Rabbitt, "Electric impedance spectroscopy using microchannels with integrated metal electrodes," *J. Microelectromech. Syst*., vol. 8, pp. 50–57, 1999.

[8] C. Iliescu, D. P. Poenar, M. Carp and F. C. Loe, "A microfluidic device for impedance spectroscopy analysis of biological samples," *Sensors Actuators* B: *Chem*., vol. 123, pp. 168–176, 2007.

[9] B. P. Cahill, A. T. Giannitsis, R. Land, G. Gastrock, U. Pliquett, D. Frense, M. Min and D. Beckmann, "Reversible Electrowetting on Silanized Silicon Nitride," *Sensors Actuators* B: *Chem*., vol. 144, pp. 380–386, 2010.

[10] J. T. Schumacher, A. Grodrian, C. Kremin, M. Hoffmann and J. Metze, "Hydrophobic coating of microfluidic chips structured by SU-8 polymer for segmented flow operation," *J. Micromech. Microeng*., vol. 18, pp. 055019, 2008.

[11] R. Pintelon, J. Schoukens, *System identification: a frequency domain approach*. Piscataway, NJ, USA: IEEE Press, 2001.

[12] K. Godfrey, *Perturbation signals for system identification*. Hertfordshire, UK: Prentice-Hall International, 1993.

[13] M. Friese, "Multitone signals with low crest factor," *IEEE Trans on Communications*, vol. 45, no. 10: pp. 1338–1344, 1997.

[14] D. Rees, D. L. Jones, "Design and application of non-binary low peak factor signals for system dynamic measurement," in *Proc. Int. Conference on Control*, Edinburgh, UK, 1991, pp. 644-650.

[15] Y. Yang, M. Kang, Y. Lu, J. Wang, J. Yue, Z. Gao, "Design of a wideband excitation source for fast bioimpedance spectroscopy," *Measurement Science and Technology*, vol. 22, 8 pp., 2011,

[16] Y. Yang, J. Wang, Z. Gao, D. Liand J. Wang, "Waveform synthesis of multi-frequency sinusoids with 2nth primary harmonics based on Walsh functions," in *Proc. IEEE Biomedical Circuits and Systems Conference*, Bejing, China, 2009, pp. 129–132.

[17] A. v.d. Bos and R. Krol, "Synthesis of discrete-interval binary signals with specified Fourier amplitude spectra," *Int J Control*, vol. 30, pp. 871–884, 1979.